

Network localization governs social contagion dynamics with macro-level reinforcement

Leyang Xue,^{1,2,3} Kai-Cheng Yang,^{4,5} Peng-Bi Cui,^{1,2,3,*} and Zengru Di^{1,2,3}

¹*Department of Systems Science, Faculty of Arts and Sciences, Beijing Normal University, Zhuhai, 519087, China*

²*International Academic Center of Complex Systems, Beijing Normal University, Zhuhai, 519087, China*

³*School of Systems Science, Beijing Normal University, Beijing, 100875, China*

⁴*School of Computing, Binghamton University, Binghamton, NY, USA*

⁵*Network Science Institute, Northeastern University, Boston, MA, USA*

(Dated: December 18, 2025)

The spread of ideas, behaviors, and technologies generally depends on feedback mechanisms operating across multiple scales. Previous studies have extensively examined pairwise transmission and local reinforcement. However, the role of macro-level social influence—where widespread adoption enhances further adoption—remains understudied. Here, we focus on a contagion process that incorporates both pairwise interactions and macro-level reinforcement. We show that the contagion undergoes a shift from continuous to mixed-order transition as macro-level influence exceeds a reinforcement threshold. Simulations on various real-world networks indicate that network localization governs the contagion outcomes by determining the critical point and the reinforcement threshold. Building on this insight, we develop a structural metric linking network localization to contagion dynamics, revealing a key trade-off: networks that facilitate weak contagion tend to experience slower diffusion and lower adoption rates, while networks that suppress weak contagions enable faster and more widespread adoption. These findings challenge the conventional belief that stronger local connectivity uniformly promotes contagion.

I. INTRODUCTION

Contagion processes characterize the dissemination of new ideas, technologies, products, and behaviors, playing a central role in the functioning of socio-economic systems. Understanding the mechanisms underlying these processes provides key insights into collective decision-making and adoption dynamics across a wide range of disciplines [1–3], including management science, economics, sociology, psychology, and physics [4–6]. Because empirical studies often face substantial confounding factors, modeling approaches have become essential tools for analyzing and predicting social diffusion patterns [7, 8]. Network science offers a principled framework to examine contagion pathways and uncover the mechanisms driving emergent collective behaviors in diffusion processes [9, 10].

Classical contagion models typically assume pairwise transmission with a constant and independent probability between susceptible and adopting individuals [11, 12]. However, real adoption behaviors frequently require reinforcement from multiple exposures before individuals commit to new behaviors [13–16]. This has motivated the development of threshold models [17], simplicial and higher-order contagion models [3, 18], and hypergraph-based frameworks [19]. These models primarily emphasize the role of local reinforcement through interacting neighborhoods [58], communities [20, 21], simplices, or

hyperedges [3, 18, 19, 22, 23], in producing nonlinear adoption patterns.

However, the rise of digital communication, large-scale media exposure, and platform-driven recommendation systems has amplified the influence of macro-level social signals on individual adoption decisions. Empirical studies have documented abrupt increases in adoption rates driven by visibility, popularity, and network effects at the population scale [24–26, 29, 30]. Examples include the rapid spread of online platforms such as Facebook, Twitter, and Threads [25, 27, 28], as well as viral dissemination of digital content and AI tools [31, 32]. These dynamics highlight that the global fraction of adopters can directly reinforce micro-level transmission, thereby creating a positive feedback loop that accelerates adoption.

Macro-level reinforcement can arise from various mechanisms, including psychological conformity to emerging social norms [16, 33–35], network effects that enhance product utility in large user bases [36–38], and cost reductions driven by economies of scale [8, 39, 40]. Regardless of its origins, such system-level reinforcement couples the global state of adoption back into local transmission dynamics. Capturing this macro–micro interaction requires a modeling framework that integrates global reinforcement with local contagion processes while accounting for underlying network structure, a connection that remains insufficiently explored in existing contagion models.

To close this gap, we develop a model that captures the interplay between macro-level reinforcement and local pairwise transmission, incorporating varying levels of feedback intensity. The contagion process is mod-

* cuiisir610@gmail.com

eled using a Susceptible-Infectious-Recovered (SIR)-like framework [11], where word-of-mouth effects [41] drive initial adoption. Macro-level influence is represented as the increasing adoption likelihood as the total number of adopters grows. Specifically, transmissibility β' is defined by two key components: (1) the inherent initial attractiveness of the contagion, β , and (2) a macro-level social influence or reinforcement term $\alpha \frac{R(t)}{N}$, where $R(t)$ and N denote the number of adopters and the total population size, respectively, and α represents the feedback strength.

Simulations on diverse real-world networks reveal a critical threshold in inherent attractiveness, β_c , below which outbreaks cannot occur. When macro-level influence exceeds a critical value α_c (i.e., the reinforcement threshold), the outbreak size at β_c exhibits an abrupt jump associated with critical scaling behavior. This indicates that sufficiently strong global feedback transforms gradual diffusion into an abrupt mixed-order (hybrid) transition.

We identify α_c as the onset of mixed-order criticality and show that it is closely tied to network localization strength, providing a clear structural interpretation. To quantify this relationship, we propose a localization metric that predicts α_c directly from network topology and reveals a fundamental trade-off: for networks with fixed density, lowering β_c inevitably raises α_c , and vice versa. Consequently, strongly localized networks can trigger contagion with low intrinsic attractiveness but restrict the final adoption size, whereas weakly localized networks require higher intrinsic attractiveness yet can sustain a much broader spread.

Our findings challenge classical diffusion theory, which posits that networks with high degree heterogeneity or strong clustering are optimal for lowering contagion thresholds. Instead, we show that such structural features can localize spreading dynamics and restrict global outbreaks, especially when macro-level reinforcement interacts with network localization. By bridging micro-level transmission and macro-level reinforcement, our framework provides a unified perspective on how network structure shapes diffusion dynamics, offering new strategies for both promoting beneficial adoption and mitigating undesirable contagion.

II. MODEL

Consider a socio-economic system represented as a network of N individuals (nodes) connected by L links (edges). Initially, most nodes are in a susceptible state (denoted by S) and can transition to an adopter state (denoted by A) when influenced by neighboring adopters. The adoption occurs with a probability β' , representing the reinforced transmission probability along local connections. Additionally, adopters may lose interest and transition to a recovered state (denoted by R) with probability μ per time step. The contagion dynamics are de-

scribed as follows:

$$S_i(t-1) + A_j(t-1) \xrightarrow{\beta'(t)} A_i(t) + A_j(t), \quad (1)$$

$$A_i(t-1) \xrightarrow{\mu} R_i(t), \quad (2)$$

where $Y_i(t)$ ($Y \in \{S, A, R\}$) denotes the state of node i at time t . Local transmission occurs only between directly connected nodes i and j . The contagion process stops once all adopters have transitioned to the recovered state.

To incorporate macro-level reinforcement [33, 46, 47], we adopt a linear feedback mechanism inspired by the classical Bass diffusion model [7], where the adoption rate increases linearly with the cumulative number of adopters. This formulation is supported by empirical studies [1, 7, 34], which report approximately linear increases in adoption likelihood during the early and intermediate stages of diffusion. Although real-world reinforcement mechanisms may display nonlinear effects such as thresholds or saturation, this linear approximation provides a parsimonious yet empirically grounded representation that captures the core features of macro-level reinforcement while maintaining analytical tractability for exploring the role of network structure in contagion dynamics.

Specifically, the time-dependent transmissibility β' is defined as:

$$\beta'(t) = \min \left(1, \beta + \alpha \frac{R(t-1)}{N} \right), \alpha \geq 0, \beta' \in [0, 1]. \quad (3)$$

Here, β represents the intrinsic attractiveness of the contagion [1], while $\alpha \frac{R(t-1)}{N}$ captures the macro-level influence from cumulative adoption. As $R(t-1)$ increases, the probability that a susceptible individual adopts also increases, reflecting the reinforcing effect of collective behavior. The parameter α controls the level of feedback intensity, and the upper bound ensures that $\beta'(t)$ remains within the valid probability range. An overview of the model is illustrated in Fig. 1(a).

III. RESULT

A. Phase Transition

To characterize the behavior of our model, we perform simulations across a range of β and α values on various real-world networks. Results for three representative networks are shown in Fig. 1(b). Additionally, we apply the dynamic message passing (DMP) method to theoretically track the final market penetration, i.e., $\frac{R(\infty)}{N}$. The theoretical predictions exhibit strong agreement with simulation results. The simulation procedures and the DMP method are described in Appendices A and C, respectively, while information on the network datasets and additional results is provided in the Supplemental Material [48].

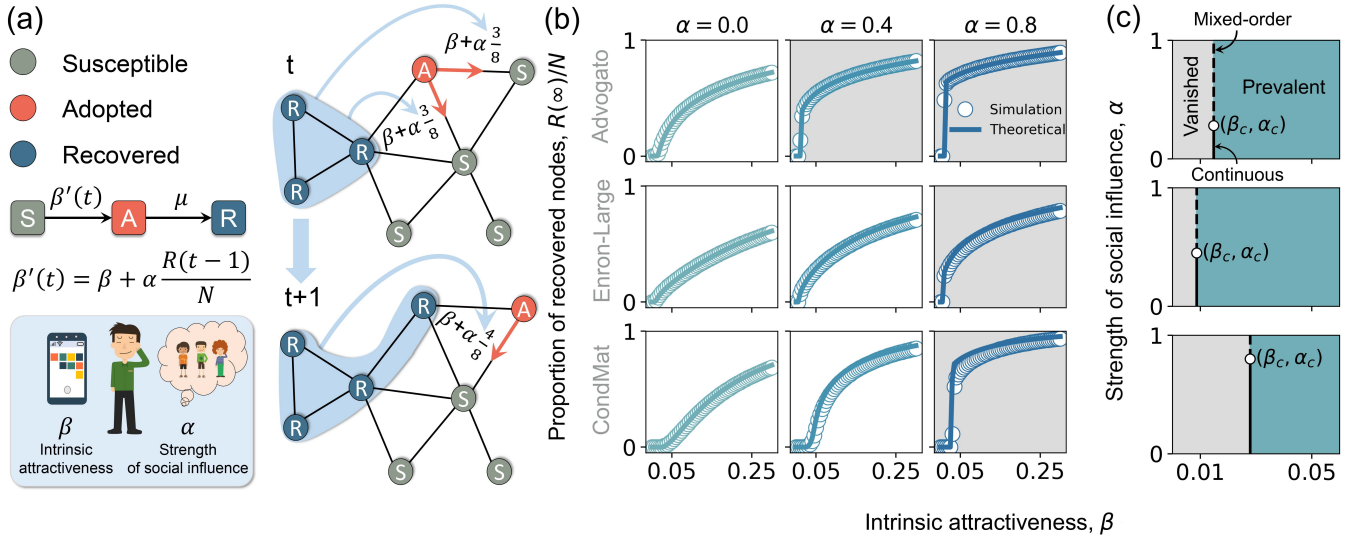


FIG. 1. **Definition and behavior of the proposed model.** (a) The diagram depicts the contagion process within a simplified network consisting of eight nodes. The transmissibility, $\beta'(t)$, of the SIR-like model depends on both intrinsic attractiveness, β , and macro-level reinforcement, $\alpha \frac{R(t-1)}{N}$. At time t , an adopter tries to convert two susceptible neighbors, with the macro-level influence contribution to transmissibility being $\alpha \frac{3}{8}$, since there are three recovered nodes in the system. At time $t+1$, the level of feedback intensity rises to $\alpha \frac{4}{8}$ due to the addition of one more recovered node. (b) The final proportion of recovered nodes, $R(\infty)/N$, is depicted as a function of β for three different values of α across three real-world networks (Advogato, Enron-Large, and CondMat networks). Dots represent simulation results, while solid lines denote theoretical predictions derived from the dynamic message passing (DMP) method. As the level of feedback intensity increases, the contagion exhibits a finite jump in the outbreak size, as indicated by the gray backgrounds. Additional details are provided in the main text. (c) Phase diagrams for the same networks as in (b) are divided by a vertical line at the critical point β_c , separating the “vanished” and “prevalent” contagion states. In the former state, the contagion decays, while in the latter state, it spreads widely. Solid lines ($\alpha < \alpha_c$) indicate continuous transitions, while dashed curves ($\alpha > \alpha_c$) indicate transitions that develop a finite jump in outbreak size. The white dot marks the value of α_c at which this qualitative change in transition behavior occurs.

Through extensive analysis, we identify key phenomena that shed light on the contagion process. In the absence of macro-level reinforcement (i.e., $\alpha = 0$), our model reduces to the classical SIR model. As β surpasses a critical threshold β_c , the system undergoes a continuous transition from the “vanished” state, where contagion fails to spread, to the “prevalent” state, where a finite fraction of individuals eventually adopt. The introduction of macro-level reinforcement fundamentally alters these dynamics. When this feedback strength is sufficiently high, the final adoption size at β_c exhibits an abrupt jump, while still displaying critical scaling behavior near the critical point (see Supplemental Material [49], Sec. B.2).

This qualitative change reflects the emergence of a mixed-order transition, in which an abrupt jump coexists with critical behavior rather than a purely first-order transition. In particular, the intrinsic threshold β_c remains unchanged across different values of α (see Supplemental Material [50], Sec. B.3), since macro-level reinforcement only becomes operative once adopters already exist, requiring $\beta \geq \beta_c$ for contagion to spread initially.

We further identify a reinforcement threshold, α_c , beyond which contagion exhibits a mixed-order phase transition (see plots with gray backgrounds in Fig. 1(b)) [51,

52]. We refer to this threshold as the onset of mixed-order criticality and provide a numerical estimation method in Appendix D. The model’s behavior is thus characterized by the tuple (β_c, α_c) , which partitions the phase space into distinct regions, as shown in Fig. 1(c). These thresholds have important real-world implications: β_c represents the intrinsic attractiveness required to trigger an outbreak, while α_c determines the level of feedback intensity needed to induce an abrupt but hybrid global adoption surge. Networks with lower α_c values generally exhibit faster diffusion and higher adoption rates (see Supplemental Material [53], Sec. B.1).

B. Quantifying the critical point and reinforcement threshold of phase transition

Given the critical roles of β_c (the critical point) and α_c (the reinforcement threshold), accurately estimating their values is essential to understand contagion dynamics in networked populations. While these thresholds can be determined numerically, the process requires extensive simulations, making it prohibitively expensive (see Appendix A for details). Here, we demonstrate that both β_c and α_c are inherently determined by the network struc-

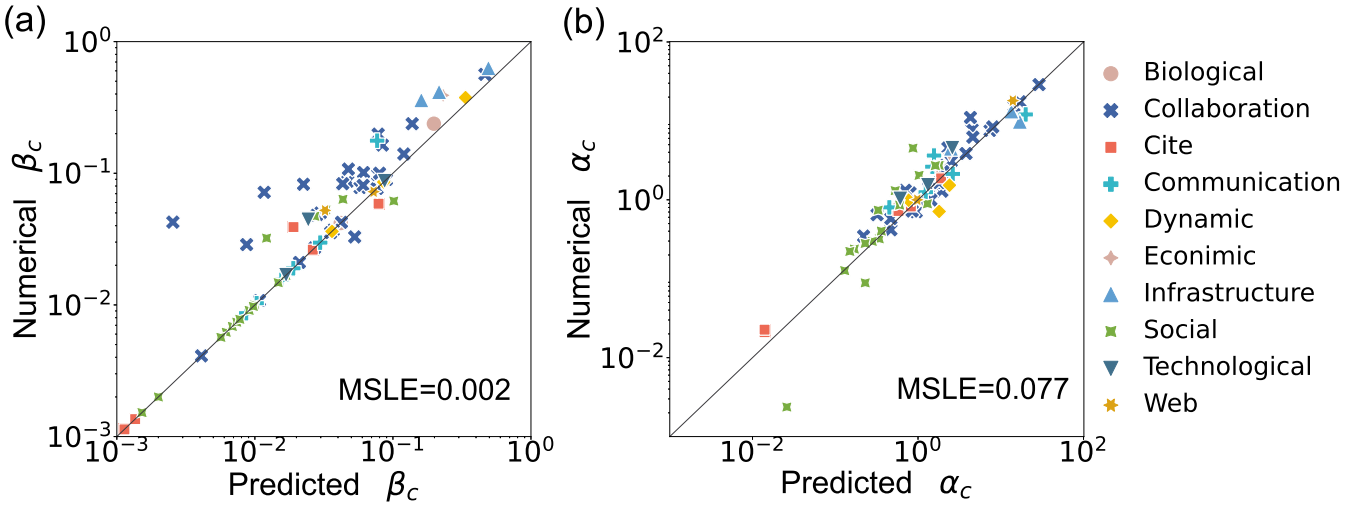


FIG. 2. **Critical point (β_c) and reinforcement threshold (α_c) for real-world networks.** (a) Comparison between simulated and predicted values of β_c , based on Eq. (4). (b) Comparison between simulated and predicted values of α_c , derived from Eq. (7). Each dot represents a real-world network, and the solid diagonal lines ($y = x$) indicate where predicted values match simulated results. The mean squared logarithmic errors (MSLE) between simulations and predictions are annotated in each plot.

ture and can be efficiently calculated using simple algebraic expressions derived from the non-backtracking matrix [45].

In the previous section, we established that the simulated value of β_c is independent of the macro-level feedback. Therefore, it can be approximated by the epidemic threshold of the SIR model [54]:

$$\beta_c = \frac{\mu}{\rho(B) + \mu - 1}, \quad (4)$$

where $\rho(B)$ is the largest eigenvalue of the non-backtracking matrix B . For simplicity, we set $\mu = 1$, yielding a threshold approximation of $1/\rho(B)$. To validate this approximation, we compare the predicted and simulated values of β_c across 74 real-world networks, as shown in Fig. 2(a). The results demonstrate a strong agreement, with minor deviations consistent with previous reports [56].

The case for α_c is more complex. When macro-level reinforcement is sufficiently strong, the final adoption size at β_c exhibit a finite jump, reflecting an avalanche-like activation of susceptible individuals once β surpasses the threshold. This abrupt collective response arises when a positive feedback loop forms between the increasing number of adopters and the reinforced transmissibility β' . However, the presence of macro-level reinforcement alone is insufficient to produce such behavior. For an avalanche to occur, a substantial fraction of individuals must have similar adoption probabilities, enabling many of them to become activated nearly simultaneously. These probabilities vary across individuals due to differences in network connectivity [11, 57, 58]. For example, well-connected individuals are more likely to be exposed to contagion and adopt compared to those

with fewer connections. Previous studies suggest that adoption probability can be approximated using the non-backtracking centrality [59, 60], defined as:

$$x_i = \sum_j A_{ij} v_{j \rightarrow i}, \quad (5)$$

where x_i represents the centrality of node i , A_{ij} is an element of the adjacency matrix A , and $v_{j \rightarrow i}$ denotes the component of the principal eigenvector associated with the non-backtracking matrix B .

Based on this heuristic, mixed-order transition behavior is more likely to occur in networks with smaller variances in their node centrality measures. To illustrate this, we present diffusion outcomes on two synthetic networks in Fig. 3. While these networks share the same degree sequence, differences in their connectivity patterns result in distinct non-backtracking centrality distributions, the reinforcement threshold α_c , and final states. In particular, the network in Fig. 3(a) has a small subset of highly central nodes, while the rewired network in Fig. 3(b) displays a more homogeneous centrality distribution. By definition, network (a) has stronger localization strength than network (b). Consequently, in network (a), recovered nodes tend to be more central, with diffusion concentrated around highly connected nodes, whereas in network (b), contagion spreads more evenly across the network.

To quantify this property, we define the localization strength \mathcal{L} as:

$$\mathcal{L} = \frac{\sqrt{\frac{1}{N} \sum_{i=1}^N (x_i - \langle x_i \rangle)^2}}{\langle x_i \rangle \langle k \rangle}, \quad (6)$$

where the numerator represents the standard deviation

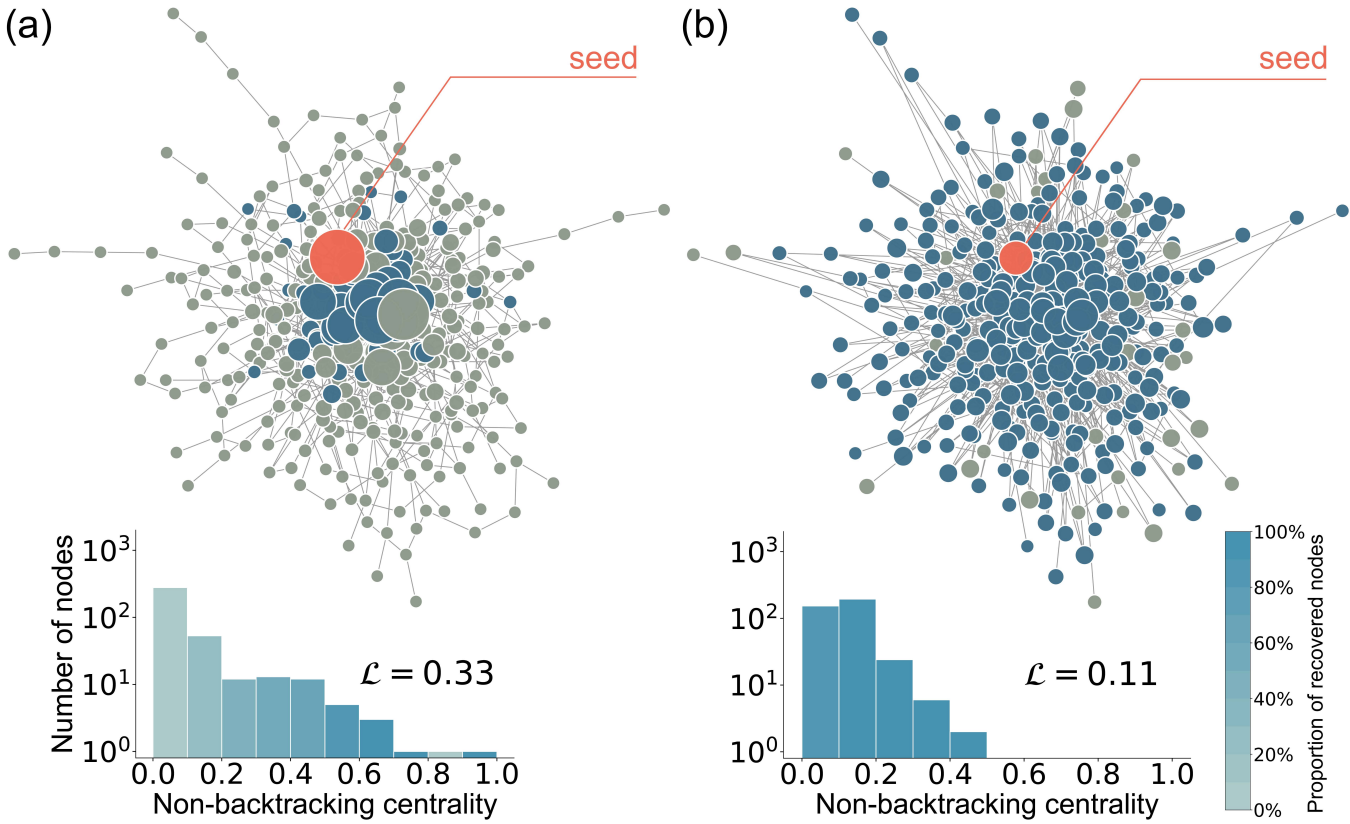


FIG. 3. Effect of network localization on the contagion process. We simulate the proposed model with the parameters $\alpha = 1$ and $\beta = \beta_c$ (the theoretical critical value) on two synthetic networks, shown in (a) and (b), respectively. The network in (b) is generated by randomly rewiring the edges of the real-world network in (a), while preserving its degree sequence. Node sizes correspond to non-backtracking centrality, with gray nodes indicating the final susceptible states and blue nodes indicating the final recovered states; the initial seed is marked in orange. The histograms display the distribution of node non-backtracking centrality indices, with each bar's color reflecting the proportion of recovered nodes within the respective bin. The figure also includes annotations for the localization metric, \mathcal{L} , for both networks. For the critical thresholds, we observe $\beta_c = 0.104$, and $\alpha_c = 1.17$ for network (a), and $\beta_c = 0.183$, $\alpha_c = 0.58$ for network (b).

of node non-backtracking centrality measures. The denominator, given by the product of the average centrality and the average degree, ensures comparability of \mathcal{L} across different networks. The value of \mathcal{L} for both networks in Fig. 3 illustrates how this metric quantifies localization strength.

By analyzing the values of \mathcal{L} and α_c across different networks, we observe a positive correlation between them, which we capture with the empirical relationship:

$$\alpha_c = \lambda \mathcal{L}^\eta, \quad (7)$$

where λ and η are parameters determined empirically. To avoid overfitting on real-world networks, we fit Eq. (7) using a collection of synthetic networks, resulting in $\lambda = 2.63$ and $\eta = 1.00$ (see Appendix D for details). We then validate this relationship by comparing the simulated α_c values with their predicted counterparts, $2.63\mathcal{L}$, across our collection of real-world networks in Fig. 2(b), finding excellent agreement. This relationship enables prediction of α_c for any network based solely on its topology, eliminating the need for extensive simulations. For

practical applications, Eq. (7) can also be fitted directly on specific real-world networks to refine the estimates of λ and η .

We acknowledge that alternative methods exist for quantifying network localization strength. For instance, the inverse participation ratio (IPR) is widely used in the literature for this purpose [45]. Other measures include substituting x_i in Eq. (6) with eigenvector centrality [61], or using the Gini coefficient to measure the variance [62]. However, our definition in Eq. (6) provides the most accurate predictions for α_c (see Supplemental Material [63], Sec. B.4 for a comparison with alternative definitions).

Beyond predicting the reinforcement threshold, Eq. (7) allows us to analytically examine the relationship between β_c and α_c . For random uncorrelated networks, we have the following relationship:

$$\beta_c = \frac{1}{\langle k \rangle^3 (\alpha_c / \lambda)^{2/\eta} + \langle k \rangle - 1}, \quad (8)$$

where the average degree $\langle k \rangle$ quantifies the network's edge density (see Appendix E for the derivation of

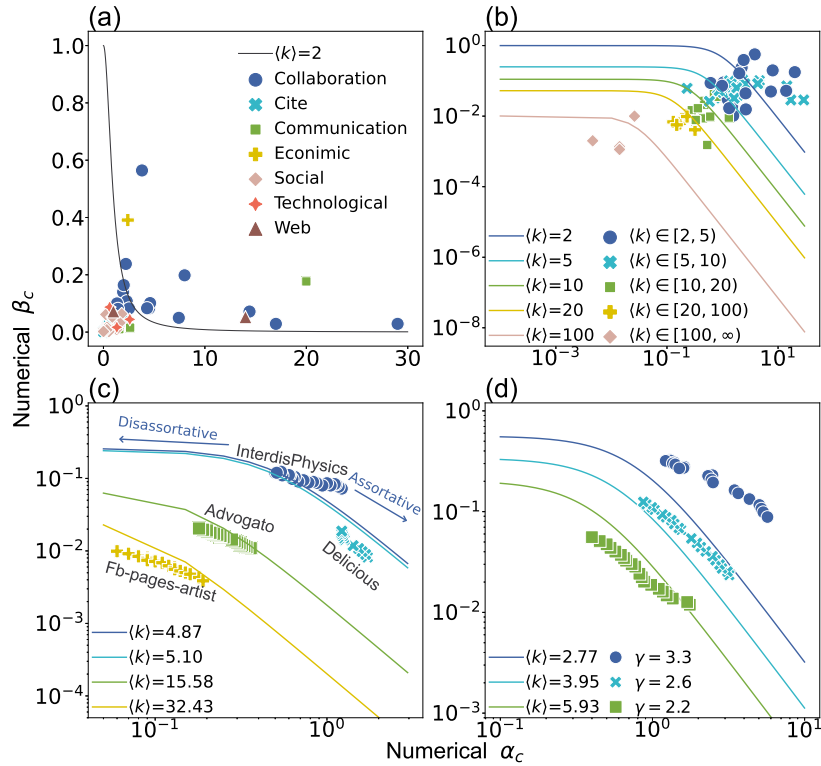


FIG. 4. **Relationship between the critical point and the reinforcement threshold.** Values of β_c and α_c are obtained through numerical simulations. Each marker represents a network, with its position indicating the corresponding intrinsic threshold and reinforcement threshold. Solid lines illustrate the relationship between β_c and α_c as described by Eq. (8) for the specified average degree. (a) Equation (8) is plotted with $\langle k \rangle = 2$. (b) Networks are categorized by average degree, with lines representing different $\langle k \rangle$ values. A logarithmic scale is used to highlight finer details. (c) Adjusting network assortativity yields configurations with varying β_c and α_c values for four selected real-world networks (InterdisPhysics, Delicious, Advogato, Fb-pages-artist). Arrows indicate the directions of these changes. (d) Similar to (c), but applied to three scale-free networks generated by the configuration model.

Eq. (8)). Since all networks considered satisfy $\langle k \rangle > 2$, Eq. (8) indicates that β_c decreases monotonically with α_c , and that higher $\langle k \rangle$ values lead to lower values of both β_c and α_c .

As previously noted, a smaller β_c allows contagion with lower attractiveness to spread, whereas a smaller α_c enables faster diffusion and higher adoption. Thus, networks with lower β_c and α_c values are generally more effective at facilitating broad diffusion. To assess real-world networks' efficacy, we plot them in the (β_c, α_c) plane in Fig. 4(a), including a reference curve from Eq. (8) with $\langle k \rangle = 2$, which serves as an upper bound. Most networks align closely with or fall below this curve, supporting our theoretical framework. Many networks cluster near the origin, suggesting that real-world networks tend to be optimized for social contagion. There are a few exceptions, primarily among collaboration networks, which may be hindered by cultural or knowledge transfer [64].

To better visualize these relationships, Fig. 4(b) reproduces Fig. 4(a) using a logarithmic scale, incorporating troughs from Eq. (8) with varying $\langle k \rangle$ values and color-coded markers representing network average de-

grees. Most networks fall within the predicted troughs, validating our theory on the relationship between the intrinsic threshold β_c and the reinforcement threshold α_c . As shown earlier, β_c and α_c regulate the contagion processes: to maximize the number of adopters, one would need to minimize both of them. However, Eq. (8) suggests that this is only achievable by increasing the density of the networks (i.e., adding new connections). When the network density is fixed, Eq. (8) introduces a trade-off: increasing localization strength (larger \mathcal{L}) would reduce β_c but increase α_c , and vice versa.

Under this constraint, we show that rewiring the network while preserving edge density can adjust the values of β_c and α_c . A particularly effective method is the Xulvi-Brunet–Sokolov algorithm [65], which modifies the localization strength by tuning network assortativity (see Supplemental Material [66], Sec. B.7). Increasing assortativity enhances localization strength, raising α_c while lowering β_c . Figure 4(c) illustrates this effect on four networks, confirming that Eq. (8) holds. This approach extends to synthetic networks, as shown in Fig. 4(d). Additionally, scatter plots of the predicted α_c and β_c values exhibit patterns consistent with Fig. 4, further validating

ing our theoretical framework regarding the relationship between them (see Supplemental Material [67], Sec. B.6).

IV. DISCUSSION

In this paper, we present a comprehensive analysis of a contagion process that explicitly couples micro-level pairwise transmission with macro-level positive feedback. Without macro-level reinforcement, the system undergoes a continuous transition from a vanished state to a prevalent state as the intrinsic attractiveness of the contagion increases. Once the reinforcement strength exceeds a threshold α_c , the final outbreak size exhibits an abrupt jump that is nevertheless accompanied by critical behavior, a hallmark of mixed-order criticality. This demonstrates the profound impact of macro-level reinforcement on contagion dynamics.

To contextualize these findings within the broader landscape of contagion research, we note that abrupt or explosive epidemic growth has been observed in other irreversible spreading models, including those driven by higher-order interactions [42] and collapse phenomena in limited-resource detection processes [43]. In these systems, strongly nonlinear outbreak curves emerge even though the underlying phase transition remains continuous. Our work complements these studies by revealing a distinct mechanism that produces mixed-order transitions—characterized by an abrupt order-parameter jump accompanied by critical behavior—through the interplay between global reinforcement and structural localization.

Based on this insight, we identify network localization strength as a key structural factor governing the onset of mixed-order behavior. To quantify this property, we introduce the metric \mathcal{L} , derived from non-backtracking centrality, which captures heterogeneity in node-level infection probabilities for percolation-like (irreversible) dynamics. By accounting for path redundancy and avoiding overcounting from short cycles, \mathcal{L} enables accurate prediction of the reinforcement threshold α_c directly from network topology. Its predictive power stands in contrast to classical localization measures such as the inverse participation ratio (IPR) [44], which were designed for linear SIS processes and are less suited to percolation-like contagion with feedback. Across diverse networks, \mathcal{L} consistently outperforms IPR and other localization metrics in estimating α_c . Its algebraic simplicity also suggests its potential applicability to other dynamical processes on networks.

Beyond predicting the onset of mixed-order behavior, \mathcal{L} also reveals a quantitative relationship between the intrinsic critical point β_c and the reinforcement threshold α_c . This relationship provides a practical framework for evaluating and optimizing contagion efficiency in socio-economic systems. When promoting contagion, low values of both thresholds are desirable and can be facilitated by increasing network edge density. When edge density

is fixed, however, a fundamental trade-off emerges: lowering one threshold inevitably raises the other. Consequently, highly attractive contagions benefit from targeting populations with large β_c (and thus smaller α_c), while less attractive contagions can still achieve global spread in populations with lower β_c , albeit more gradually.

Finally, although our analysis focuses on linear macro-level reinforcement, real contagion processes often involve nonlinear forms of global influence, including thresholds, saturation, and diminishing returns. Linear reinforcement nevertheless serves as a standard first-order approximation that maintains analytical tractability while exposing the fundamental interaction between feedback and topology. Therefore, this framework establishes a solid foundation for future extensions incorporating nonlinear reinforcement functions in networked diffusion systems.

ACKNOWLEDGMENTS

This work was supported by the Key Program of the National Natural Science Foundation of China (Grant No. 71731002), and by the Guangdong Basic and Applied Basic Research Foundation (Grant Nos. 2024A1515012692). Leyang Xue acknowledges the support of the China Scholarship Council Program and the Israeli Sandwich Scholarship. The authors thank Claudio Castellano for the helpful comments and suggestions.

Appendix A: Numerical simulations

In each realization, one node is randomly assigned the A (adopter) state to initiate the diffusion process, while all other nodes are set to the S (susceptible) state. The diffusion then proceeds according to the model rules until it reaches an absorbing state, where no further transmission is possible. Throughout this study, the recovery probability μ is fixed at 1 for simplicity.

In our model, the critical point β_c is determined numerically by identifying the maximum value of susceptibility, defined as

$$\chi = \frac{\sqrt{\langle r(\infty)^2 \rangle - \langle r(\infty) \rangle^2}}{\langle r(\infty) \rangle}. \quad (\text{A1})$$

To ensure reliability, we perform 10^4 independent realizations to compute the first and second moments of $r(\infty)$ for a given network under identical parameters.

To determine α_c , we classify phase transitions by examining the mass distribution of $r(\infty)$ at the predicted β_c values, varying α across numerous independent realizations. Abrupt transitions are identified by the appearance of an isolated peak representing giant recovered clusters [57]. Additional details and illustrative examples are provided in the Supplemental Material [68], Sec. B.5.

Appendix B: Non-backtracking matrix and non-backtracking centrality

Given the central role of the non-backtracking matrix in our theoretical analysis, we provide a brief introduction here. In an undirected network with L edges, the non-backtracking matrix B is a $2L \times 2L$ non-symmetric matrix in which rows and columns correspond to directed edges $j \rightarrow i$, representing edges directed from node j to node i . The elements of B are defined as follows:

$$B_{z \rightarrow i, j \rightarrow z'} = \begin{cases} 1 & \text{if } z' = z, j \neq i, \\ 0 & \text{otherwise.} \end{cases} \quad (\text{B1})$$

When all nodes in the network belong to a strongly connected giant component, the non-backtracking matrix is non-negative and irreducible. According to the Perron-Frobenius theorem [69], there exists a positive leading eigenvector $v_{j \rightarrow i}$ associated with the largest eigenvalue λ_B :

$$\lambda_B v_{j \rightarrow i} = \sum_{k \rightarrow m} B_{j \rightarrow i, k \rightarrow m} v_{k \rightarrow m}. \quad (\text{B2})$$

The element $v_{j \rightarrow i}$ of this leading eigenvector represents the centrality of node j , excluding any influence from node i . The non-backtracking centrality of node i is then defined as:

$$x_i = \sum_j A_{ij} v_{j \rightarrow i}. \quad (\text{B3})$$

Unlike eigenvector centrality, non-backtracking centrality mitigates the “self-inflating” effect associated with hub nodes [45, 56].

Appendix C: Dynamic Message Passing method

To analytically determine the outbreak size and threshold, we use the dynamic message passing (DMP) method. DMP is widely applied in contagion studies as it prevents backtracking to the source node, thereby avoiding mutual transmission effects [54, 70, 71]. This method effectively predicts the probability of each node being in a given state at time t , particularly in tree-like networks, and is robust to various initial conditions.

First, we derive the exact equations that govern the DMP method. Let $P_S^i(t)$, $P_A^i(t)$, and $P_R^i(t)$ denote the probabilities of node i being in the susceptible (S), adopted (A), or recovered (R) state at time t , respectively. These probabilities satisfy the following constraint:

$$P_A^i(t) + P_S^i(t) + P_R^i(t) = 1. \quad (\text{C1})$$

The recovery of an adopted node i occurs independently, regardless of its neighbors’ states. Therefore, the

probability of node i being in the recovered state at time t , denoted $P_R^i(t)$, is given by:

$$P_R^i(t) = P_R^i(t-1) + \mu P_A^i(t-1), \quad (\text{C2})$$

where μ is the fixed recovery probability. To find the overall fraction of recovered nodes in the network at time t , we sum $P_R^i(t)$ across all nodes:

$$R(t) = \sum_{i=1}^N P_R^i(t). \quad (\text{C3})$$

Inserting Eq. (C3) into Eq. (3) yields:

$$\beta'(t) = \min \left(1, \beta + \alpha \frac{\sum_{i=1}^N P_R^i(t-1)}{N} \right), \quad (\text{C4})$$

where $\beta'(t)$ increases with $R(t-1)$ until it reaches a maximum value of 1.

For a susceptible node i , the probability of remaining in the susceptible state up to time t , denoted $P_S^i(t)$, can be described as:

$$P_S^i(t) = P_S^i(0) \Phi_i(t), \quad (\text{C5})$$

where $\Phi_i(t)$ is the probability that node i has not received successful transmissions from any adopted neighbors by time t . The DMP approach assumes that the network is tree-like, so each neighbor of node i ’s evolves independently. However, if node i is influenced by a neighbor node z and switches to the adopted state (A), it may attempt to influence another neighbor node z' . This interdependence introduces a challenge, as the transitions of nodes z and z' become correlated once i adopts the contagion.

To address this issue, we assume that the focal node i is in a cavity state and define $\theta^{z \rightarrow i}(t)$ as the probability that node i has not been successfully influenced by node z up to time t . Consequently, $\Phi_i(t)$ can be factorized as $\prod_{z \in \partial i} \theta^{z \rightarrow i}(t)$, where ∂i represents the set of neighbors of node i . Substituting this expression into Eq. (C5) gives:

$$P_S^i(t) = P_S^i(0) \prod_{z \in \partial i} \theta^{z \rightarrow i}(t). \quad (\text{C6})$$

In message-passing, directionality is preserved, meaning that $\theta^{i \rightarrow z}(t) \neq \theta^{z \rightarrow i}(t)$ in undirected networks. We treat each undirected edge as two directed edges pointing in opposite directions. Initially, we set $\theta^{z \rightarrow i}(0) = 1$ for all edges in the network. As time progresses, $\theta^{z \rightarrow i}(t-1)$ decreases as the contagion is transmitted from node z to node i with probability $\beta'(t) \phi^{z \rightarrow i}(t-1)$, where $\phi^{z \rightarrow i}(t-1)$ represents the probability that the adopted node z has not yet passed the contagion to node i by time $t-1$. Accordingly, $\theta^{z \rightarrow i}(t)$ updates according to the rule:

$$\theta^{z \rightarrow i}(t) = \theta^{z \rightarrow i}(t-1) - \beta'(t) \phi^{z \rightarrow i}(t-1). \quad (\text{C7})$$

To derive the expression for $\phi^{z \rightarrow i}(t)$, we first recognize that $\phi^{z \rightarrow i}(t)$ decreases when node z (currently in

the adopted state A) recovers, or it transmits the contagion to node i , or both events occur simultaneously. The probabilities for these events are μ , $\beta'(t)$, and $\mu\beta'(t)$, respectively. Additionally, $\phi^{z \rightarrow i}(t)$ can increase if node z , originally in the susceptible state S , switches to the adopted state A . The rate of this change, $\Delta P_S^{z \rightarrow i}(t)$,

$$\begin{aligned}\phi^{z \rightarrow i}(t) &= \phi^{z \rightarrow i}(t-1) - \beta'(t)\phi^{z \rightarrow i}(t-1) - \mu\phi^{z \rightarrow i}(t-1) + \mu\beta'(t)\phi^{z \rightarrow i}(t-1) \\ &\quad + P_S^{z \rightarrow i}(t-1) - P_S^{z \rightarrow i}(t) \\ &= (1 - \beta'(t))(1 - \mu)\phi^{z \rightarrow i}(t-1) + P_S^{z \rightarrow i}(t-1) - P_S^{z \rightarrow i}(t).\end{aligned}\quad (\text{C8})$$

Next, we need to explicitly define $P_S^{z \rightarrow i}(t)$. Since we are treating node i as a cavity, node z will remain susceptible as long as it is not influenced by any of its neighbors other than i . Using Eq. (C6), the probability that node z remains susceptible while i is a cavity is given by:

$$P_S^{z \rightarrow i}(t) = P_S^z(0) \prod_{j \in \partial z \setminus i} \theta^{j \rightarrow z}(t), \quad (\text{C9})$$

where $\partial z \setminus i$ represents the set of neighbors of z , excluding i . At $t = 0$, we set the initial condition as $P_S^{z \rightarrow i}(0) = 1$ if z is not the initial adopter, and $P_S^{z \rightarrow i}(0) = 0$ if z is the seed node. This can be compactly represented by $P_S^{z \rightarrow i}(0) = 1 - \delta_{q_z(0), A}$, where $\delta_{q_z(0), A}$ is the Kronecker delta function indicating the initial state of node z .

Using Eqs. (C4), (C7)-(C9), we can finally compute the trajectories of $\theta^{z \rightarrow i}(t)$, $\phi^{z \rightarrow i}(t)$, and $P_S^{z \rightarrow i}(t)$, starting with the following initial conditions:

$$\theta^{z \rightarrow i}(0) = 1, \quad (\text{C10})$$

$$\phi^{z \rightarrow i}(0) = P_A^z(0) = \delta_{q_z(0), A}, \quad (\text{C11})$$

$$P_S^{z \rightarrow i}(0) = P_S^z(0) = 1 - \delta_{q_z(0), A}. \quad (\text{C12})$$

Additionally, by incorporating the initial conditions $P_R^i(0) = 0$ and $\beta'(0) = \beta$ into Eqs. (C1), (C2), (C4), and (C6)-(C9), we can compute the complete trajectories of $P_S^i(t)$, $P_A^i(t)$, $P_R^i(t)$, ultimately determining the order parameter $R(\infty)$. The DMP approach used here has a computational complexity of $O(L)$, where L denotes the number of edges in the network.

Appendix D: Relationship between reinforcement threshold and localization strength

To characterize the relationship between the localization strength \mathcal{L} and α_c , we begin by calculating their values across various network models and real-world networks (see Supplemental Material [55], Sec. A.2) and visualizing them. We observe that α_c increases linearly with \mathcal{L} on a logarithmic scale, suggesting a relationship of the form $\ln \alpha_c = \eta \ln \mathcal{L} + \delta$, or equivalently, $\alpha_c = \lambda \mathcal{L}^\eta$, where $\lambda = e^\delta$. The parameters η and δ are estimated from the

can be expressed as the difference between the probabilities of node z remaining susceptible at consecutive times, i.e., $P_S^{z \rightarrow i}(t-1) - P_S^{z \rightarrow i}(t)$. Here, $P_S^{z \rightarrow i}(t)$ represents the probability of node z remaining in state S after interacting with the node i in the cavity state. Combining these elements, we have:

data. To avoid overfitting the real-world networks, we apply the least squares method to fit this relationship to a set of network models, yielding $\eta = 1.00$ and $\lambda = 2.63$. Therefore, we have $\alpha_c = 2.63\mathcal{L}$. This relationship allows us to estimate α_c based on network topology.

Appendix E: Relationship between critical point and reinforcement threshold

With the analytical expressions of α_c and β_c , we can now explore their relationship. In uncorrelated random networks, the components of the leading eigenvector in the non-backtracking matrix are determined by node degrees, as expressed in Eq. (E1) [56],

$$v_{j \rightarrow i} \sim k_j - 1. \quad (\text{E1})$$

Using this approximation, we can represent the non-backtracking centrality for node i as:

$$x_i = \sum_j A_{ij} v_{j \rightarrow i} \sim \sum_j \frac{k_i k_j}{N \langle k \rangle} (k_j - 1) = \frac{\langle k^2 \rangle - \langle k \rangle}{\langle k \rangle} k_i, \quad (\text{E2})$$

where we replace A_{ij} by its expectation in annealed networks, $\hat{A}_{ij} = \frac{k_i k_j}{N \langle k \rangle}$. The first moment of x_i then becomes:

$$\langle x_i \rangle = \frac{\sum_i x_i}{N} \sim \langle k^2 \rangle - \langle k \rangle. \quad (\text{E3})$$

Substituting Eqs. (E2) and (E3) into the expression for localization strength, Eq. (6), we obtain:

$$\mathcal{L} = \frac{\sqrt{\langle k^2 \rangle - \langle k \rangle^2}}{\langle k \rangle^2}. \quad (\text{E4})$$

This result shows that \mathcal{L} depends solely on the first- and second-order moments of $\langle k \rangle$. Similarly, in annealed networks [56], β_c can be written as:

$$\beta_c = \frac{\langle k \rangle}{\langle k^2 \rangle - \langle k \rangle}. \quad (\text{E5})$$

Combining Eqs. (E4) and (E5), we have:

$$\beta_c = \frac{1}{\langle k \rangle^3 \mathcal{L}^2 + \langle k \rangle - 1}. \quad (\text{E6})$$

Finally, by incorporating the relationship $\alpha_c = \lambda \mathcal{L}^\eta$, we can express β_c in terms of α_c :

$$\beta_c = \frac{1}{\langle k \rangle^3 (\alpha_c / \lambda)^{2/\eta} + \langle k \rangle - 1}. \quad (\text{E7})$$

DATA AVAILABILITY

All data supporting this study are available on Mendeley Data (<https://data.mendeley.com/datasets/d848h7rcdg>) and are described in detail in the Supplemental Material [72].

[1] Everett M Rogers. *Diffusion of innovations*. New York: The Free Press, 2003.

[2] Johan Ugander, Lars Backstrom, Cameron Marlow, and Jon Kleinberg. Structural diversity in social contagion. *Proc. Natl. Acad. Sci. U.S.A.*, 109(16):5962–5966, 2012.

[3] Iacopo Iacopini, Giovanni Petri, Alain Barrat, and Vito Latora. Simplicial models of social contagion. *Nat. Commun.*, 10(1):2485, 2019.

[4] Rabik Ar Chatterjee and Jehoshua Eliashberg. The innovation diffusion process in a heterogeneous population: A micromodeling approach. *Manage Sci*, 36(9):1057–1079, 1990.

[5] Frances Stokes Berry and William D Berry. Innovation and diffusion models in policy research. *Theories of the policy process*, pages 253–297, 2018.

[6] Gabriel E. Kreindler and H. Peyton Young. Rapid innovation diffusion in social networks. *Proc. Natl. Acad. Sci.*, 111:10881–10888, 2014.

[7] Frank M Bass. A new product growth for model consumer durables. *Manage Sci*, 15(5):215–227, 1969.

[8] Elmar Kiesling, Markus Günther, Christian Stummer, and Lea M Wakolbinger. Agent-based simulation of innovation diffusion: a review. *Cent Eur J Oper Res*, 20(2):183–230, 2012.

[9] Giulia Cencetti, Diego Andrés Contreras, Marco Mancastrappa, and Alain Barrat. Distinguishing simple and complex contagion processes on networks. *Phys. Rev. Lett.*, 130(24):247401, 2023.

[10] Yichuan Jiang and J. C. Jiang. Diffusion in social networks: A multiagent perspective. *IEEE Trans. Syst. Man Cybern. Syst.*, 45(2):198–213, 2014.

[11] Romualdo Pastor-Satorras, Claudio Castellano, Piet Van Mieghem, and Alessandro Vespignani. Epidemic processes in complex networks. *Rev. Mod. Phys.*, 87:925–979, Aug 2015.

[12] Luís MA Bettencourt, Ariel Cintrón-Arias, David I Kaiser, Carlos Castillo-Chávez. The power of a good idea: Quantitative modeling of the spread of ideas from epidemiological models. *Physica A*, 364:513–536, 2006.

[13] Damon Centola and Michael Macy. Complex contagions and the weakness of long ties. *American Journal of Sociology*, 113(3):702–734, 2007. The University of Chicago Press.

[14] Damon Centola. The spread of behavior in an online social network experiment. *Science*, 329(5996):1194–1197, 2010.

[15] Damon Centola. *How Behavior Spreads: The Science of Complex Contagions*. Volume 3. Princeton University Press, Princeton, NJ, 2018.

[16] Douglas Guilbeault, Joshu Becker, and Damon Centola. *Complex Contagions: A Decade in Review*, pages 3–25. Springer International Publishing, Cham, 2018.

[17] Duncan J Watts. A simple model of global cascades on random networks. *Proc. Natl. Acad. Sci. U.S.A.*, 99(9):5766–5771, 2002.

[18] Sandeep Chowdhary, Aanjaneya Kumar, Giulia Cencetti, Iacopo Iacopini, and Federico Battiston. Simplicial contagion in temporal higher-order networks. *J. Phys. Complex.*, 2(3):035019, 2021.

[19] Guilherme Ferraz de Arruda, Giovanni Petri, and Yamir Moreno. Social contagion models on hypergraphs. *Phys. Rev. Res.*, 2(2):023032, 2020.

[20] Zhen Su, Wei Wang, Lixiang Li, H. Eugene Stanley, and Lidia A. Braunstein. Optimal community structure for social contagions. *New J. Phys.*, 20(5):053053, 2018.

[21] Guillaume St-Onge, Iacopo Iacopini, Vito Latora, Alain Barrat, Giovanni Petri, Antoine Allard, and Laurent Hébert-Dufresne. Influential groups for seeding and sustaining nonlinear contagion in heterogeneous hypergraphs. *Commun. Phys.*, 5(1):25, 2022.

[22] Guilherme Ferraz de Arruda, Giovanni Petri, Pablo Martín Rodríguez, and Yamir Moreno. Multistability, intermittency, and hybrid transitions in social contagion models on hypergraphs. *Nat. Commun.*, 14(1):1375, 2023.

[23] Guilherme Ferraz de Arruda, Alberto Aleta, and Yamir Moreno. Contagion dynamics on higher-order networks. *Nat. Rev. Phys.*, 6(8):468–482, 2024.

[24] Jukka-Pekka Onnela and Felix Reed-Tsochas. Spontaneous emergence of social influence in online systems. *Proc. Natl. Acad. Sci.*, 107(43):18375–18380, 2010.

[25] Jameson L. Toole, Meeyoung Cha, and Marta C. González. Modeling the adoption of innovations in the presence of geographic and media influences. *PLoS One*, 7(1):e29528, 2012.

[26] Zhenfeng Ma, Zhiyong Yang, and Mehdi Mourali. Consumer adoption of new products: Independent versus interdependent self-perspectives. *J. Mark.*, 78(2):101–117, 2014.

[27] Haewoon Kwak, Changhyun Lee, Hosung Park, and Sue Moon. What is Twitter, a social network or a news media? In *Proceedings of the 19th International Conference on World Wide Web*, pages 591–600, April 2010.

[28] Fabio Duarte. Number of ChatGPT Users (Nov 2024). Exploding Topics, November 12, 2024. Accessed November 13, 2024. <https://explodingtopics.com/blog/chatgpt-users>.

[29] Wenjing Duan, Bin Gu, and Andrew B. Whinston. Informational cascades and software adoption on the internet: an real-world investigation. *MIS Quarterly*, pages 23–48,

2009.

[30] Hyeon Jo and Youngsok Bang. Analyzing ChatGPT adoption drivers with the TOEK framework. *Sci. Rep.*, 13(1):22606, 2023.

[31] Soroush Vosoughi, Deb Roy, and Sinan Aral. The spread of true and false news online. *Science*, 359(6380):1146–1151, 2018.

[32] V. Kumar, Abdul R. Ashraf, and Waqar Nadeem. AI-powered marketing: What, where, and how? *Int. J. Inf. Manag.*, 77:102783, 2024.

[33] Daire McCoy and Seán Lyons. Consumer preferences and the influence of networks in electric vehicle diffusion: An agent-based microsimulation in ireland. *Energy Res. Soc. Sci.*, 3:89–101, 2014.

[34] H Peyton Young. Innovation diffusion in heterogeneous populations: Contagion, social influence, and social learning. *Am Econ Rev*, 99(5):1899–1924, 2009.

[35] Ching-Wen Chen, Hung-Yi Chang, Juin-Han Chen, and Richard Weng. Elucidating the role of conformity in innovative smartphones. *Int. J. Mob. Commun.*, 14(1):56–78, 2016.

[36] Michael L. Katz and Carl Shapiro. Product introduction with network externalities. *J Ind Econ*, 40(1):55–83, 1992.

[37] Detlef Schoder. Forecasting the success of telecommunication services in the presence of network effects. *Inf. Econ. Policy*, 12(2):181–200, 2000.

[38] Jeffrey H Rohlfs. *Bandwagon effects in high-technology industries*. MIT press, 2003.

[39] Frederic M Scherer and David Ross. Industrial market structure and economic performance. *University of Illinois at Urbana-Champaign's Academy for entrepreneurial leadership historical research reference in entrepreneurship*, 1990.

[40] Edgar K Browning and Mark A Zupan. *Microeconomics: Theory and applications*. John Wiley & Sons, 2020.

[41] Francis A Buttle. Word of mouth: understanding and managing referral marketing. *J. Strateg. Mark.*, 6(3):241–254, 1998.

[42] F. Malizia, A. Guzmán, I. Iacopini, and I. Z. Kiss. Disentangling the role of heterogeneity and hyperedge overlap in explosive contagion on higher-order networks. *Phys. Rev. Lett.*, 135(20):207401, 2025.

[43] S. Lamata-Otíñ, A. Reyna-Lara, D. Soriano-Paños, V. Latora, and J. Gómez-Gardeñes. Collapse transition in epidemic spreading subject to detection with limited resources. *Phys. Rev. E*, 108(2):024305, 2023.

[44] A. V. Goltsev, S. N. Dorogovtsev, J. G. Oliveira, and J. F. F. Mendes. Localization and spreading of diseases in complex networks. *Phys. Rev. Lett.*, 109:128702, Sep 2012.

[45] Travis Martin, Xiao Zhang, and M. E. J. Newman. Localization and centrality in networks. *Phys. Rev. E*, 90:052808, Nov 2014.

[46] Catherine SE Bale, Nicholas J McCullen, Timothy J Foxon, Alastair M Ruckridge, and William F Gale. Harnessing social networks for promoting adoption of energy technologies in the domestic sector. *Energy Policy*, 63:833–844, 2013.

[47] Sebastiano A Delre, Wander Jager, Tammo HA Bijmolt, and Marco A Janssen. Will it spread or not? the effects of social influences and network topology on innovation diffusion. *J Prod Innov Manage*, 27(2):267–282, 2010.

[48] See Supplemental Material at [URL] for details on the network datasets and additional numerical results.

[49] See Supplemental Material at [URL] for details on the mixed-order (hybrid) phase transition and the associated scaling analyses (Sec. B.2).

[50] See Supplemental Material at [URL] for details on the effect of macro-level reinforcement on the intrinsic threshold β_c (Sec. B.3).

[51] S Boccaletti, JA Almendral, S Guan, I Leyva, Z Liu, I Sendiña-Nadal, Z Wang, and Y Zou. Explosive transitions in complex networks' structure and dynamics: Percolation and synchronization. *Phys. Rep.*, 660:1–94, 2016.

[52] Raissa M D’Souza, Jesus Gómez-Gardeñes, Jan Nagler, and Alex Arenas. Explosive phenomena in complex networks. *Adv. Phys.*, 68(3):123–223, 2019.

[53] See Supplemental Material at [URL] for details on the implications of the reinforcement threshold α_c (Sec. B.1).

[54] Andreas Koher, Hartmut H. K. Lentz, James P. Gleeson, and Philipp Hövel. Contact-based model for epidemic spreading on temporal networks. *Phys. Rev. X*, 9:031017, Aug 2019.

[55] See Supplemental Material at [URL] for details on the network models (Sec. A.2).

[56] Romualdo Pastor-Satorras and Claudio Castellano. The localization of non-backtracking centrality in networks and its physical consequences. *Sci. Rep.*, 10(1):1–12, 2020.

[57] Weiran Cai, Li Chen, Fakhteh Ghanbarnejad, and Peter Grassberger. Avalanche outbreaks emerging in cooperative contagions. *Nat. Phys.*, 11(11):936–940, 2015.

[58] Peng-Bi Cui, Wei Wang, Shi-Min Cai, Tao Zhou, Ying-Cheng Lai, et al. Close and ordinary social contacts: How important are they in promoting large-scale contagion? *Phys. Rev. E*, 98(5):052311, 2018.

[59] Munik Shrestha, Samuel V Scarpino, and Christopher Moore. Message-passing approach for recurrent-state epidemic models on networks. *Phys. Rev. E*, 92(2):022821, 2015.

[60] G. Timár, S. N. Dorogovtsev, and J. F. F. Mendes. Localization of nonbacktracking centrality on dense subgraphs of sparse networks. *Phys. Rev. E*, 107:014301, Jan 2023.

[61] Phillip Bonacich. Factoring and weighting approaches to status scores and clique identification. *J Math Sociol.*, 2(1):113–120, 1972.

[62] RB Bendel, SS Higgins, JE Teberg, and DA Pyke. Comparison of skewness coefficient, coefficient of variation, and gini coefficient as inequality measures within populations. *Oecologia*, 78(3):394–400, 1989.

[63] See Supplemental Material at [URL] for a comparison of different approaches to quantify the localization strength and their performance in predicting α_c (Sec. B.4).

[64] Margaret L Sheng, Shen-Yao Chang, Thompson Teo, and Yuh-Feng Lin. Knowledge barriers, knowledge transfer, and innovation competitive advantage in healthcare settings. *Manag. Decis.*, 51(3):461–478, 2013.

[65] R. Xulvi-Brunet and I. M. Sokolov. Reshuffling scale-free networks: From random to assortative. *Phys. Rev. E*, 70:066102, Dec 2004.

[66] See Supplemental Material at [URL] for details on tuning the localization strength of networks (Sec. B.7).

[67] See Supplemental Material at [URL] for an analysis of the relation between the predicted critical threshold β_c and the reinforcement threshold α_c (Sec. B.6).

- [68] See Supplemental Material at [URL] for details on identifying the class of phase transitions (Sec. B.5).
- [69] Roger A Horn and Charles R Johnson. *Matrix analysis*. Cambridge university press, 2012.
- [70] Brian Karrer and M. E. J. Newman. Message passing approach for general epidemic models. *Phys. Rev. E*, 82:016101, Jul 2010.
- [71] Andrey Y. Lokhov, Marc Mézard, Hiroki Ohta, and Lenka Zdeborová. Inferring the origin of an epidemic with a dynamic message-passing algorithm. *Phys. Rev. E*, 90:012801, Jul 2014.
- [72] See Supplemental Material at [URL] for detailed descriptions of the data used in this study.
- [73] Ryan A. Rossi and Nesreen K. Ahmed. The network data repository with interactive graph analytics and visualization. In *AAAI*, 2015.
- [74] Krzysztof J Cios and Lukasz A Kurgan. Trends in data mining and knowledge discovery. In *Advanced techniques in knowledge discovery and data mining*, pages 1–26. Springer, 2005.
- [75] Vladimir Batagelj and Andrej Mrvar. Analysis of large networks. In *Proceedings of Pajek Workshop at XXVI Sunbelt Conference*, 2006.
- [76] Jure Leskovec and Andrej Krevl. SNAP Datasets: Stanford large network dataset collection. <http://snap.stanford.edu/data>, June 2014.
- [77] Albert-László Barabási. *Network Science*. Cambridge University Press, 2016.
- [78] K.-I. Goh, B. Kahng, and D. Kim. Universal behavior of load distribution in scale-free networks. *Phys. Rev. Lett.*, 87:278701, Dec 2001.
- [79] B. Gross, I. Bonamassa, and S. Havlin. Fractal fluctuations at mixed-order transitions in interdependent networks. *Phys. Rev. Lett.*, 129(26):268301, 2022.
- [80] I. Bonamassa, B. Gross, J. Kertész, and S. Havlin. Hybrid universality classes of systemic cascades. *Nat. Commun.*, 16:1415, 2025.
- [81] J. Korbel, S. Havlin, and S. Thurner. Microscopic origin of abrupt mixed-order phase transitions. *Nat. Commun.*, 16:2628, 2025.
- [82] A. Bunde and S. Havlin. *Fractals and disordered systems*. Springer, 2012.
- [83] A. Bar and D. Mukamel. Mixed-order phase transition in a one-dimensional model. *Phys. Rev. Lett.*, 112(1):015701, 2014.
- [84] D. Stauffer and A. Aharony. *Introduction to percolation theory*. (Taylor & Francis, 2018).
- [85] D. Zhou, A. Bashan, R. Cohen, Y. Berezin, N. Shnerb, and S. Havlin. Simultaneous first- and second-order percolation transitions in interdependent networks. *Phys. Rev. E*, 90(1):012803, 2014.
- [86] B. Gross, I. Volotsenko, Y. Sallem, N. Yadid, I. Bonamassa, S. Havlin, and A. Frydman. The random cascading origin of abrupt transitions in interdependent systems. *Nat. Commun.*, 16:5869, 2025.
- [87] D. Dilmoney, B. Gross, S. Havlin, and N. M. Shnerb. Dynamics of critical cascades in interdependent networks. *Phys. Rev. Lett.*, 134(18):187401, 2025.